A Postsynthetic Approach for the Rational Design of Chiral Ferroelectric Metal-Organic Frameworks

Marta Mon,[†] Jesús Ferrando-Soria,[†] Michel Verdaguer,[⊥] Cyrille Train,[‡] Charles Paillard,[§] Brahim Dkhil,[§] Carlo Versace,[¶] Rosaria Bruno,[♣] Donatella Armentano*[,♣] and Emilio Pardo*[,†]

[†]Instituto de Ciencia Molecular (ICMol), Universidad de Valencia, 46980 Paterna, Valencia, Spain

[⊥]Institut Parisien de Chimie Moléculaire, Université Pierre et Marie Curie-Paris 6, UMR CNRS 7201, 75252 Paris cedex 05, France

[‡]Laboratoire National des Champs Magnétiques Intenses, UPR CNRS 3228, Université Grenoble-Alpes, B.P. 166, 38042 Grenoble cedex 9, France

[§]Laboratoire Structures, Propriétés et Modélisation des Solides, CentraleSupélec, CNRS-UMR 8580, Université Paris-Saclay, 92295 Châtenay-Malabry cedex, France

[¶]Dipartimento di Fisica, Università della Calabria, Rende 87036, Cosenza, Italy

[♣]Dipartimento di Chimica e Tecnologie Chimiche (CTC), Università della Calabria, Rende 87036, Cosenza, Italy

Supporting Information Placeholder

ABSTRACT: Ferroelectrics (FEs) are materials of paramount importance with a wide diversity of applications. Herein, we propose a postsynthetic methodology for the smart implementation of ferroelectricity in chiral molecule-based FEs: following a single-crystal to single-crystal cation metathesis, the Ca^{2+} counterions of a preformed chiral Metal-Organic Framework (MOF) of formula $Ca_6^{II}\{Cu^{II}_{24}[(S,S)\text{-hismox}]_{12}(OH_2)_3\} \cdot 212H_2O$ (**1**), where hismox is a chiral ligand derived from the natural amino acid L-histidine, are replaced by $CH_3NH_3^+$. The resulting compound, $(CH_3NH_3)_{12}\{Cu^{II}_{24}[(S,S)\text{-hismox}]_{12}(OH_2)_3\} \cdot 178H_2O$ (**2**), retains the polar space group of **1** and is ferroelectric below 260 K. These results open a new synthetic avenue to enlarge the limited number of FE MOFs.

Ferroelectric (FE) materials,[1,2] show a spontaneous electric polarization that can be switched by an external electric field *E*. They attract much interest as they can find a wide variety of important applications.[2] Most of FE materials synthesized so far[3–8] have been identified by a benchmark of the materials crystalizing in polar space groups, compatible with ferroelectricity. However, the development of more rational synthetic methodologies targeting such materials is still challenging.

Metal-Organic Frameworks (MOFs)[9] appear as good candidates to reach this goal: they are porous crystalline materials that exhibit both, a large diversity of captivating high-dimensional (porous) structures and exciting properties.[10] The uniqueness of MOFs resides on the possibility to combine a precise determination of their crystal structure and a rich host-guest chemistry.[10] So, MOFs are, *a priori*, the perfect playgrounds to carry out a *molecular approach* for the synthesis of molecule-based FEs or multiferroics (MFs).[11,12]

Nonetheless, the global strategy based on the direct synthesis of MOFs with flexible open-framework structures capable to host and align in their void spaces the dipolar guest molecules usually required to develop ferroelectricity has only led to a limited number of FE[13–17] and/or MF[18–24] MOFs. This limited efficiency is related to the necessary conditions to observe ferroelectricity such as a large polarizability of the guest molecules (although ferroelectricity can be also observed using nonpolar molecules in certain circumstances[1]) and a polar space group[4].

Aiming to overcome such current synthetic limitations, we propose a programmed postsynthetic strategy[25] for the rational design of FE materials. The first step of this approach is the selection of a MOF with the appropriate polar space group. The second step is a solid-state single-crystal to single-crystal (SC to SC) process allowing to insert, into the preformed MOF, molecules with a strong dipolar moment *P*. The polar space group of the MOF would actually impose a non-centrosymmetric organization of the molecules, avoiding the cancellation of the macroscopic polarization most often observed during the direct crystallization of polar molecules.[26]

Herein, the selected *polar* MOF is a novel chiral oxamidato-based[27–29] *bio*MOF, of formula $Ca_6^{II}\{Cu^{II}_{24}[(S,S)\text{-hismox}]_{12}(OH_2)_3\} \cdot 212H_2O$ (**1**) [H_2Me_2-(*S,S*)-hismox = bis[(*S*)-histidine]oxalyl diamide, Scheme S1a]. The dipolar molecule is the versatile $CH_3NH_3^+$. The process is a solid-state postsynthetic[25] metathesis, where the Ca^{2+} cations are replaced by the polar $CH_3NH_3^+$ ones, which are known to be favorable for FE.[22] It yields a new MOF of formula $(CH_3NH_3)_{12}\{Cu^{II}_{24}[(S,S)\text{-hismox}]_{12}(OH_2)_3\} \cdot 178H_2O$ (**2**) (see Experimental section). It preserves the polar space group of **1** (see structural section), and creates the appropriate environment for the polar $CH_3NH_3^+$ cations and opens the gate for the observation of ferroelectric properties. This post-synthetic strategy appears

a rational method towards molecular FE materials giving, *a priori*, highest chances to observe FE properties.

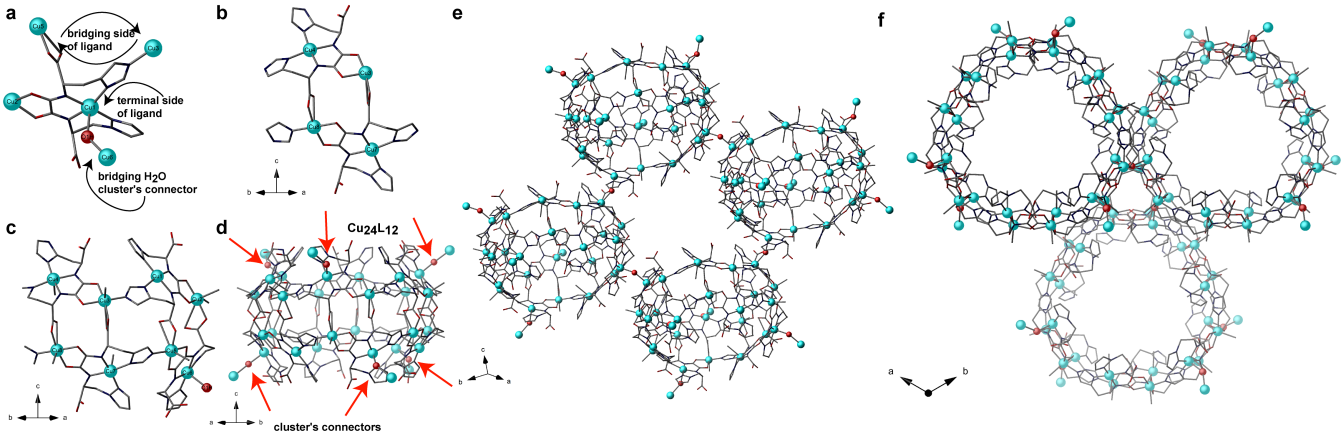

Figure 1. a) Perspective view of a fragment of the crystal structure of **1** showing the coordination mode of [(*S,S*)-hismox]$^{5-}$ ligand. (b,c) Interlocked *cis* oxamidato-bridged dicopper(II) {Cu^{II}_2[(*S,S*)-hismox]} units. (d) Perspective view of a {Cu^{II}_{24}[(*S,S*)-hismox]$_{12}$(OH_2)$_3$} *basket-like* cage along [1 1 1] direction with arrows underlining bridging water molecules as *connectors* of the framework. Lateral (e) and frontal (f) views of connected cages generating the 3D chiral porous network. Copper atoms are represented by cyan spheres whereas organic ligands are depicted as sticks. The bridging water molecules are shown here as red spheres. Free water molecules and Ca^{2+} ions residing in the cages are omitted for clarity.

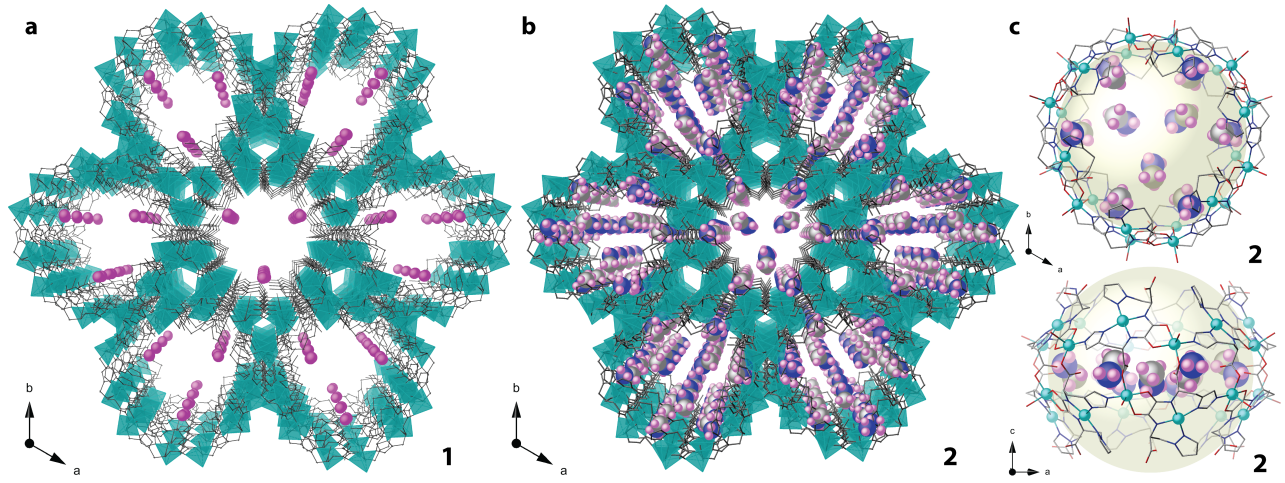

Figure 2. Perspective views along the *c* axis of the porous structures of **1** (a) and **2** (b) showing the replacement of the Ca^{2+} cations (purple spheres) by the $CH_3NH_3^+$ ones (N: blue, C: gray; H: pink). Copper atoms are represented by cyan polyhedra whereas organic ligands are depicted as sticks. (c) Perspective views along the *c* (top) and *b* (bottom) axes of the Cu_{24} baskets containing the $CH_3NH_3^+$ cations. The copper(II) ions are shown here as cyan spheres. Free water molecules are omitted for clarity.

The crystal structures of **1** and **2** could be determined by single-crystal X-ray diffraction (see Experimental Section, Supporting Information). **1** and **2** are isomorphous and crystallize in the polar *R*3 space group. For **1**, the observation of a chiral space group is insured by the use of hismox, a ligand derived from the chiral pool, whereas the preservation of the space group during the metathesis proves the validity of the first step in our design strategy (Table S1). The structure of both MOFs reveals an infinite network of huge basket-like cages featuring a narrow window with a van der Waals diameter of *ca.* 16 Å and an effective cage size of 22 Å (Figures 1-2 and S1). The cages are built by twenty-four Cu(II) metal ions and twelve hismox ligands (Figures 1d, S1-S2), which are further interconnected through bridging water molecules yielding a 3D chiral highly porous network. The pillared cages generate either pseudo-hexagonal nanosized channels of 1.4 nm or smaller hexagonal or trigonal ones (of *ca.* 0.5 and 0.4 nm, respectively) along the [001] direction (Figures 1e,f, 2 and S3-S9), with effective calculated void volumes of 70.6 (**1**) and 70% (**2**). Both structures unfold an unprecedented binodal 3,4-connected net with stoichiometry (3-c)(4-c) and point symbol for net {4^2.6.12^3}{4^2.6} (Figures S10 and S11).[30]

In **1**, each cage hosts dinuclear $[Ca_2(\mu\text{-}H_2O)_2(H_2O)_8]^{4+}$ units and water molecules (Figures 2a and S5-S6), whereas in **2** $CH_3NH_3^+$ guest cations are placed in both the basket-like cages and the interstitial voids between them (Figures 2b,c and S7-S9). The $[Ca_2(\mu\text{-}H_2O)_2(H_2O)_8]^{4+}$ (**1**) and $CH_3NH_3^+$ cations (**2**), located within the Cu_{24} cages (Figures 2, 3a and S5-S9), participate in a pretty intricate hydrogen-bonded network with the large amount of lattice water molecules, which could be experimentally determined, and the available imidazole groups from the ligands. In **1**, [Ca_2(μ-

$H_2O)_2(H_2O)_8]^{4+}$ dimers are bound to the net by bridging water molecules (Figures S5-S6). In contrast, in **2**, $CH_3NH_3^+$ guest cations arrangement unambiguously shows polar molecular ions grasped through H- bonds by walls of the cages, involving also coordinated carboxylic groups and coordinated water molecules. Further H-bonds involving only free water molecules stabilize other

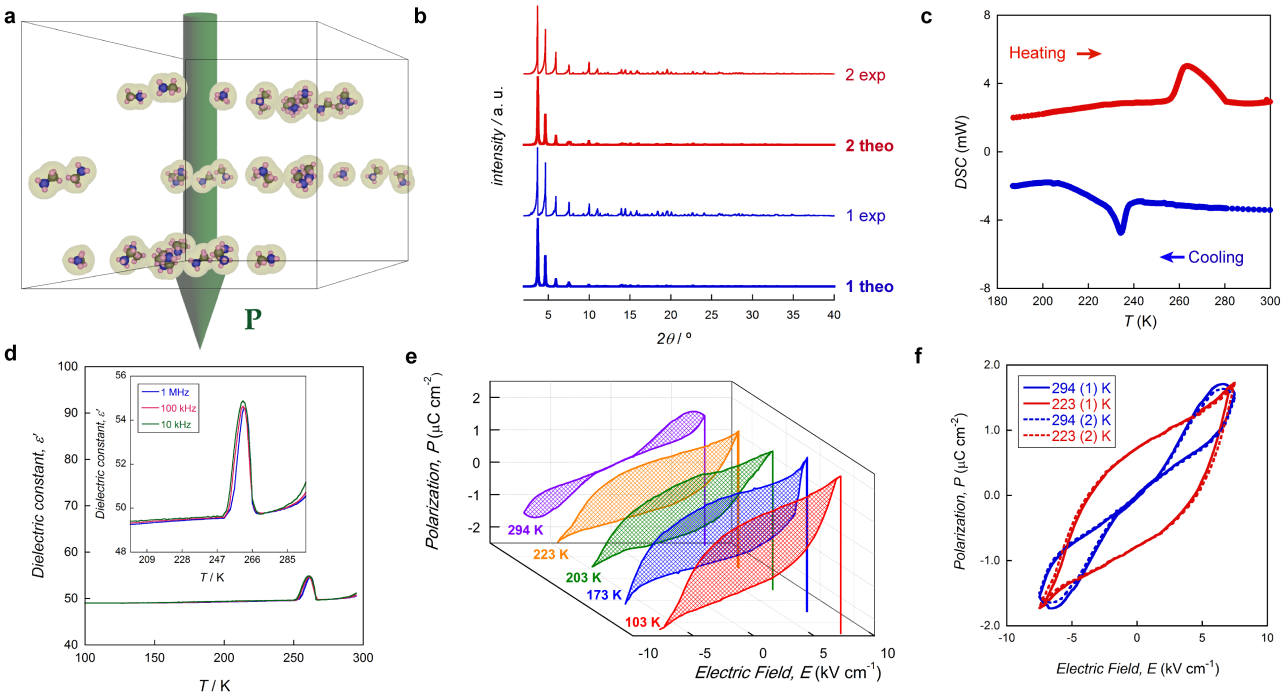

Figure 3. a) Filling of the unit cell of **2** with the $CH_3NH_3^+$ cations. The green arrow indicates the overall polar orientation along the *c* axis. b) Calculated (bold lines) and experimental (regular lines) PXRD patterns of **1** (blue) and **2** (red) in the 2θ range 2.0–40.0° at R.T. c) DSC data showing the structural transition in **2**. d) Temperature dependence of ε' for **2** measured at different frequencies. e) Polarization *vs* electric field loops of **2** as a function of temperature. Vertical lines are eye guides. f) Electric field dependence of the polarization of **2** at 294 (blue) and 223 K (red). Bold and dashed lines represent the first and second cycle, respectively.

$CH_3NH_3^+$ around the center of the cages (see Supporting Information), ensuring their cohesion and leading to a complete filling of the cage (Figures S8-S9). The arrangement of the methylammonium cations in **2** is dependent on the H-bonds directionality and on the host matrix chiral structure (Figures 2b,c and S9). The comparison of the positions of the cations in the cages of **1** and **2** suggests that the exchange of Ca^{2+} by $CH_3NH_3^+$ occurs through a molecular recognition process, most-likely directed by H-bonds involving the crystallization water molecules, and leads to a preferential insertion of the $CH_3NH_3^+$ cations in the positions predefined by the Ca^{2+} ones (Figures S5-S8).

The experimental powder X-ray diffraction (PXRD) patterns of **1** and **2** (Figures 3b, S12 and S13) confirm that the 3D anionic network does not experiment significant phase transitions between 100 (Temperature at which the crystal structures were resolved) and 298 K. However, Differential Scanning Calorimetry (DSC) measurements of **2** clearly show a heat anomaly at *ca.* 264 K upon heating and at *ca.* 235 K upon cooling (Figure 3c). This suggests a reversible first-order phase transition involving only free water molecules and $CH_3NH_3^+$ cations. Thermogravimetric analyses (TGA) confirmed the water contents provided by XRD (Figure S14).

As far as ferroelectricity is concerned, two fundamental informations derive from the structural analysis: (*i*) the polar space group *R*3 of **2** imposed by the conservation of that of **1**; (*ii*) the non-compensation of the dipolar moments of the $CH_3NH_3^+$ inserted in the voids of the structure by cation metathesis. Accordingly, **2** fulfills the constraining requirements for ferroelectricity to be present in a material. Thus, electrical measurements were performed on both **1** and **2** to ensure the identification of the origin of FE properties.

In **1**, the dielectric constant ε' showed a low and constant value of *ca.* 3, when browsing both the temperature and the frequency (Figure S15a). Moreover, no hysteresis loop in the polarization *vs.* electric field plot could be observed (Figure S15b). Overall, these electrical measurements indicate paraelectric-like characteristics, even if **1** presents a polar space group and a complex hydrogen-bonded array of water molecules that could be responsible for FE properties.[14]

In **2**, the temperature dependence of ε' in the range 100-300 K (Figure 3d), shows a constant value of *ca.* 50 in the low temperature region and a remarkable anomaly at T_C = 260 K. This feature is indicative of a dielectric phase transition[31] that matches with the structural phase transition observed by DSC (Figure 3c). Moreover, Figure 3d shows no frequency

dependence in the 1kHz-1MHz range supporting the existence of a weak conductivity, if any. Figure S16 shows the temperature dependence of the dielectric losses tan(δ) exhibiting a very low value less than 0.1% in the whole range of temperature. Polarization *vs.* Electric Field measurements were performed at different temperatures. Above T_C, a double hysteresis loop sometimes observed in FE materials above the ferroelectric-to-paraelectric transition temperature or typical of antiferroelectrics (AFEs) was observed, whereas FE hysteresis loops appear below T_C (Figure 3e). The shape of the P *vs* E loops (Figures 3e and 3f) is slightly pinched[32] at high fields, but very different from the cigar-like shape characteristic of lossy dielectrics.[33] The pinched hysteresis can be attributed to defects in the material[34] causing hardening, apparent internal fields and/or domain-wall pinning as well as to potential contribution of leakage current inducing a small extra "false" polarization. Current vs. field plots at different temperatures (Figure S17) show an ohmic behavior for **2** with resistivity of about 6.10^7 Ω.cm at 103 K which decreases when temperature increases (Figure S18) corresponding to an insulator-like behavior. Moreover while the polarization amplitude increases when the temperature decreases, the conductivity (resistivity) decreases (increases) excluding significant contribution leakage current to the polarization enhancement. Accordingly, leakage current, if any, should be negligible compared to polarization effects and the ferroelectric behavior of **2** is beyond reasonable doubt.

Since the polar state transition is associated with a structural phase one, a plausible explanation lies in a reorientation of the polar cations, most-likely associated to the thermodynamics of the H-bonded crystallization water molecules near the melting point of the H-bond network. The measurement of two consecutive cycles of P *vs*. E curves at 294 and 223 K confirmed the reversibility of the transition (Figure 3f). At 103 K, the remnant polarization value is 1.06 $\mu C.cm^{-2}$, which is rather similar to those usually observed in other molecular ferroelectrics[2] and among the highest values reported in MOFs.[15,16]

In summary, we report a dual-step synthetic methodology for the rational design of molecule-based ferroelectrics. In a first step, we synthesize a chiral metal-organic framework **1**, crystalizing in an appropriate space group. Then, a SC to SC postsynthetic cation metathesis of Ca^{2+} by $CH_3NH_3^+$ takes place. Upon cation exchange, **2** fulfills the two necessary conditions to present ferroelectricity: (*i*) a polar space group (*R*3) inherited from **1**; and (*ii*) guest molecules with large polarizability ($CH_3NH_3^+$). Accordingly, **2** exhibits a FE behavior below 260 K. These results open a route for the application of such postsynthetic chiral approach aiming at the rational obtention of novel families of ferroelectric materials.

Supporting Information

Experimental preparation, analytical and spectroscopic characterization of **1** and **2** and additional Figures S1-S19. CCDC reference numbers CCDC 1541853-1541852. This material is available free of charge via the Internet at http://pubs.acs.org.

AUTHOR INFORMATION

Corresponding Author

* To whom correspondence should be addressed. E-mail: emilio.pardo@uv.es; donatella.armentano@unical.it

Notes

The authors declare no competing financial interests.

ACKNOWLEDGMENT

This work was supported by the MINECO (Spain) (Projects CTQ2016-75671-P, the Ramón y Cajal Program (E. P.) and Excellence Unit "Maria de Maeztu" MDM-2015-0538) and the MIUR (Italy). M. M. and R. B. thank the MINECO and the MIUR (Project PON R&I FSE-FESR 2014-2020) for predoctoral contracts. MV thanks Valencia University for an invited professorship. The authors are especially grateful to Prof. Davide M. Proserpio for helpful discussions.

REFERENCES

(1) Horiuchi, S.; Tokura, Y. *Nat. Mater.* **2008**, *7*, 357.
(2) Li, J.; Liu, Y.; Zhang, Y.; Cai, H.-L.; Xiong, R.-G. *Phys. Chem. Chem. Phys.* **2013**, *15*, 20786.
(3) Busch, G. *Ferroelectrics* **1987**, *74*, 267.
(4) Khomskii, D. *Physics (College. Park. Md).* **2009**, *2*, 20.
(5) Horiuchi, S.; Tokunaga, Y.; Giovannetti, G.; Picozzi, S.; Itoh, H.; Shimano, R.; Kumai, R.; Tokura, Y. *Nature* **2010**, *466*, 1006.
(6) Leblanc, N.; Mercier, N.; Zorina, L.; Simonov, S.; Auban-Senzier, P.; Pasquier, C. *J. Am. Chem. Soc.* **2011**, *133*, 14924.
(7) Chen, S.; Zeng, X. C. *J. Am. Chem. Soc.* **2014**, *136*, 6428.
(8) Zhang, Y.; Liao, W.-Q.; Fu, D.-W.; Ye, H.-Y.; Chen, Z.-N.; Xiong, R.-G. *J. Am. Chem. Soc.* **2015**, *137*, 4928.
(9) Furukawa, H.; Cordova, K. E.; O'Keeffe, M.; Yaghi, O. M. *Science.* **2013**, *341*, 974.
(10) Cui, Y.; Li, B.; He, H.; Zhou, W.; Chen, B.; Qian, G. *Acc. Chem. Res.* **2016**, *49*, 483.
(11) Bibes, M.; Barthélémy, A. *Nat. Mater.* **2008**, *7*, 425.
(12) Scott, J. F. *Nat. Mater.* **2007**, *6*, 256.
(13) Pan, L.; Liu, G.; Li, H.; Meng, S.; Han, L.; Shang, J.; Chen, B.; Platero-Prats, A. E.; Lu, W.; Zou, X.; Li, R.-W. *J. Am. Chem. Soc.* **2014**, *136*, 17477.
(14) Dong, X.-Y.; Li, B.; Ma, B.-B.; Li, S.-J.; Dong, M.-M.; Zhu, Y.-Y.; Zang, S.-Q.; Song, Y.; Hou, H.-W.; Mak, T. C. W. *J. Am. Chem. Soc.* **2013**, *135*, 10214.
(15) Zhang, W.; Xiong, R.-G. *Chem. Rev.* **2012**, *112* (2), 1163.
(16) Asadi, K.; van der Veen, M. A. *Eur. J. Inorg. Chem.* **2016**, *2016*, 4332.
(17) Xu, G.; Ma, X.-M.; Zhang, L.; Wang, Z.; Gao, S. *J. Am. Chem. Soc.* **2010**, *132*, 9588.
(18) Gómez-Aguirre, L. C.; Pato-Doldán, B.; Mira, J.; Castro-García, S.; Señarís-Rodríguez, M. A.; Sánchez-Andújar, M.; Singleton, J.; Zapf, V. S. *J. Am. Chem. Soc.* **2016**, *138*, 1122.
(19) Di Sante, D.; Stroppa, A.; Jain, P.; Picozzi, S. *J. Am. Chem. Soc.* **2013**, *135*, 18126.
(20) Xu, G.-C.; Zhang, W.; Ma, X.-M.; Chen, Y.-H.; Zhang, L.; Cai, H.-L.; Wang, Z.-M.; Xiong, R.-G.; Gao, S. *J. Am. Chem. Soc.* **2011**, *133*, 14948.
(21) Jain, P.; Ramachandran, V.; Clark, R. J.; Zhou, H. D.; Toby, B. H.; Dalal, N. S.; Kroto, H. W.; Cheetham, A. K. *J. Am. Chem. Soc.* **2009**, *131*, 13625.
(22) Cui, H.; Wang, Z.; Takahashi, K.; Okano, Y.; Kobayashi, H.; Kobayashi, A. *J. Am. Chem. Soc.* **2006**, *128*, 15074.
(23) Fu, D.-W.; Zhang, W.; Cai, H.-L.; Zhang, Y.; Ge, J.-Z.; Xiong, R.-G.; Huang, S. D.; Nakamura, T. *Angew. Chem., Int. Ed.* **2011**, *50*, 11947.
(24) Pardo, E.; Train, C.; Liu, H.; Chamoreau, L.-M.; Dkhil, B.; Boubekeur, K.; Lloret, F.; Nakatani, K.; Tokoro, H.; Ohkoshi, S.; Verdaguer, M. *Angew. Chem., Int. Ed.* **2012**, *51*, 8356.
(25) Cohen, S. M. *J. Am. Chem. Soc.* **2017**, *139*, 2855.

(26) Stupp, S. I. *Science (80-.).* **1997**, *276*, 384.
(27) Mon, M.; Lloret, F.; Ferrando-Soria, J.; Martí-Gastaldo, C.; Armentano, D.; Pardo, E. *Angew. Chem., Int. Ed.* **2016**, *55*, 11167.
(28) Mon, M.; Ferrando-Soria, J.; Grancha, T.; Fortea-Pérez, F. R.; Gascon, J.; Leyva-Pérez, A.; Armentano, D.; Pardo, E. *J. Am. Chem. Soc.* **2016**, *138*, 7864.
(29) Grancha, T.; Ferrando-Soria, J.; Cano, J.; Amorós, P.; Seoane, B.; Gascon, J.; Bazaga-García, M.; Losilla, E. R.; Cabeza, A.; Armentano, D.; Pardo, E. *Chem. Mater.* **2016**, *28*, 4608.
(30) Blatov, V. A.; Shevchenko, A. P.; Proserpio, D. M. *Cryst. Growth Des.* **2014**, *14*, 3576.
(31) Harada, J.; Shimojo, T.; Oyamaguchi, H.; Hasegawa, H.; Takahashi, Y.; Satomi, K.; Suzuki, Y.; Kawamata, J.; Inabe, T. *Nat. Chem.* **2016**, *8*, 946.
(32) Xu, B.; Paillard, C.; Dkhil, B.; Bellaiche, L. *Phys. Rev. B* **2016**, *94*, 140101.
(33) Scott, J. F. *J. Phys. Condens. Matter* **2008**, *20*, 21001.
(34) Granzow, T.; Suvaci, E.; Kungl, H.; Hoffmann, M. J. *Appl. Phys. Lett.* **2006**, *89*, 262908.